Journal of Hazardous Materials 401 (2021) 123311

Contents lists available at ScienceDirect

Journal of Hazardous Materials

journal homepage: www.elsevier.com/locate/jhazmat

Highly efficient removal of thallium in wastewater by $MnFe_2O_4$-biochar composite

Juan Liu[a,b,*], Shixing Ren[a], Jielong Cao[a], Daniel C.W. Tsang[b], Jingzi Beiyuan[c], Yutao Peng[d], Fa Fang[a], Jingye She[a], Meiling Yin[a], Nengping Shen[e], Jin Wang[a,f,**]

[a] Key Laboratory of Water Quality and Conservation in the Pearl River Delta, Ministry of Education, Institute of Environmental Research at Greater Bay, School of Environmental Science and Engineering, Guangzhou University, Guangzhou 510006, China
[b] Department of Civil and Environmental Engineering, The Hong Kong Polytechnic University, Hung Hom, Kowloon, Hong Kong, China
[c] School of Environment and Chemical Engineering, Foshan University, Foshan, Guangdong, China
[d] Beijing Key Laboratory of Farmyard Soil Pollution Prevention-control and Remediation; College of Resources and Environmental Sciences, China Agricultural University, Beijing 100193, China
[e] State Key Laboratory of Ore Deposit Geochemistry, Institute of Geochemistry, Chinese Academy of Sciences, Guiyang 550081, China
[f] Guangdong Provincial Key Laboratory of Radionuclides Pollution Control and Resources, Guangzhou 510006, China

GRAPHICAL ABSTRACT

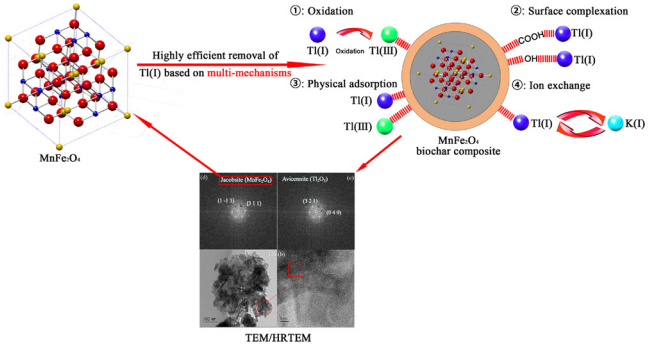

ARTICLE INFO

Editor: R Teresa.

Keywords:
Thallium remediation
Industrial wastewater treatment
Iron/manganese coprecipitation
Sustainable engineering
Engineered biochar

ABSTRACT

Thallium (Tl), is a highly toxic trace metal in the natural environment. Emerging Tl pollution in waters has gradually become a global concern. However, limited removal technologies are available for Tl-containing wastewater. Herein, $MnFe_2O_4$-biochar composite (MFBC) was successfully fabricated via coprecipitation method as a novel and efficient adsorbent for treating Tl(I)-contaminated wastewater. It was found that the MFBC, with a specific surface area of 187.03 m^2/g, exhibited high performance across a wide pH range of 4–11, with the superior Tl(I) removal capacity (170.55 mg/g) based on Langmuir model (pH 6.0, a dosage of 1 g/L). The removal mechanisms included physical and chemical adsorption, ion exchange, surface complexation, and oxidation. This investigation revealed that MFBC is a promising and environmentally friendly adsorbent with a low cost, large specific surface area, magnetic properties, and high efficiency for the removal of Tl(I) from wastewater.

* Corresponding author at: Innovation Center and Key Laboratory of Waters Safety & Protection in the Pearl River Delta, Institute of Environmental Research at Greater Bay, Guangzhou University, Guangzhou 510006, China.
** Corresponding author at: School of Environmental Science and Engineering, Guangdong Provincial Key Laboratory of Radionuclides Pollution Control and Resources, Guangzhou University, Guangzhou 510006, China.
E-mail addresses: liujuan858585@163.com (J. Liu), wangjin@gzhu.edu.cn (J. Wang).

https://doi.org/10.1016/j.jhazmat.2020.123311
Received 14 May 2020; Received in revised form 11 June 2020; Accepted 22 June 2020
Available online 25 June 2020

1. Introduction

Thallium (Tl) is an extremely toxic trace metal in the natural environment (Liu et al., 2018a; Li et al., 2017a; Xiao et al., 2012; Wang et al., 2020b; Liu et al., 2019c), whose toxicity exceeds other naturally encountered metal(loid)s such as Pb, Cd, As, and Hg (Puccini et al., 2018; George et al., 2019; Liu et al., 2019a; Wang et al., 2020c). It can lead to a variety of adverse effects on the health of most organisms, even at a low concentration, owing to its acute and chronic poisoning (Liu et al., 2018a; Vaněk et al., 2013). Therefore, Tl is listed as a dangerous pollutant by both the United States Environmental Protection Agency (EPA) and the European Union (EU) (Liu et al., 2018b). However, much less attention has been received to the Tl pollution compared with other well-recognized toxic elements, such as Cd, As, Pb, U and Hg (Liu et al., 2018b; Zhou et al., 2020; Wang et al., 2020d; Yin et al., 2020; Zhong et al., 2020; Zeng and Han, 2020). Thallium is an associated element in a variety of metal sulfide ores and coals, hence Tl pollution can be generated from wastewater discharge and solid waste from a wide range of anthropogenic activities, including mining, cement production, and smelting (Liu et al., 2018a; Tuzen et al., 2018; Saleh et al., 2018; Vanek et al., 2016; Liu et al., 2020b; Li et al., 2020). The anthropogenic release of Tl is noticeably increasing in many developing countries, causing widespread and severe human health concern (Xiao et al., 2012; Liu et al., 2020c). To control the anthropogenic discharge of Tl, a strict discharge restraint has been promulgated in China, which limits the maximum permissible level of Tl at 5 μg/L in industrial wastewaters before discharge (Li et al., 2017a).

In the natural aqueous environment, Tl has two oxidation states (Tl^{+} and Tl^{3+}), but it usually exists in Tl^{+} (Adio et al., 2019; Sabermahani et al., 2017; Liu et al., 2019b; Li et al., 2017b). Monovalent Tl is relatively mobile in aqueous solution (Liu et al., 2019b; Li et al., 2017b; Pan et al., 2014; Birungi and Chirwa, 2015). It can be replaced by K^{+} in the metabolic processes of plants due to their similar ionic radius (Liu et al., 2019a; Vanek et al., 2019; Martin et al., 2018). Trivalent Tl is analogous to Al^{3+}, which is highly reactive and can be readily hydrolyzed in the alkaline solution (Birungi and Chirwa, 2015; Liu et al., 2014a). However, due to the high redox potential of Tl^{3+}/Tl^{+} ($E^{3+}_{Tl^{3+}/Tl^{+}} = 1.28$ V), Tl is usually present in wastewaters as Tl^{+}, which is much more difficult to be removed as compared to Tl^{3+} (Wojtkowiak et al., 2016). At present, several techniques for removing

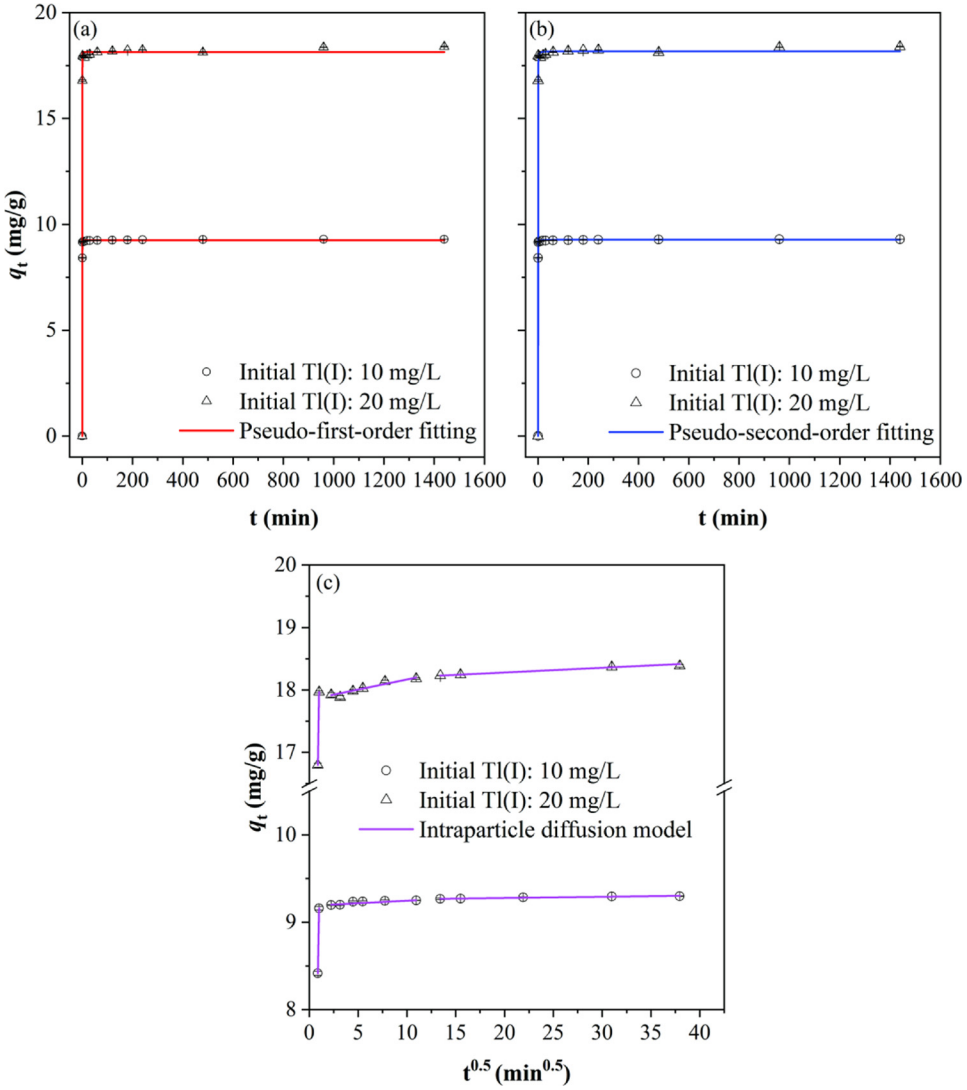

Fig. 1. Removal of Tl(I) in the initial solution of 10 and 20 mg/L by MFBC fitted with (a) Nonlinear pseudo-first-order kinetics, (b) Nonlinear pseudo-second-order kinetics, and (c) Intraparticle diffusion model.

Table 1
Parameters of Pseudo-first-order, Pseudo-second-order, and Intraparticle diffusion kinetic models for the adsorption of Tl(I) by MFBC.

Models and Parameters	MFBC	
Pseudo-first-order[a]	10 mg/L	20 mg/L
q_e	9.252	18.131
k_1	4.800	5.201
R^2	0.9998	0.9990
Pseudo-second-order		
q_e	9.280	18.181
k_2	2.533	1.552
R^2	0.9988	0.9985
Intraparticle diffusion[b]		
K_{p1}	5.757	9.071
R^2	1	1
K_{p2}	0.006	0.032
R^2	0.894	0.913
K_{p3}	0.001	0.008
R^2	0.916	0.993

[a] q_e (mg/g) refers to the removal amount of Tl on the MFBC at equilibrium, k_1 (min^{-1}) and k_2 ($g{\cdot}mg^{-1}{\cdot}min^{-1}$) are the adsorption rate parameters of pseudo-first-order and pseudo-second-order models, respectively.

[b] K_{pi} ($mg{\cdot}g^{-1}{\cdot}min^{-1/2}$) is the intraparticle diffusion rate coefficient.

Tl from wastewater have been applied, including precipitation (Vink, 1993; Peter and Viraraghavan, 2005), ion exchange (Li et al., 2017b; Albert and Masson, 1994), and adsorption (Adio et al., 2019; Huangfu et al., 2015a; Liu et al., 2014b). In numerous metal and organic pollutants removal technologies, adsorption is extensively regarded as a promising one, due to its high efficiency, simplicity, and low cost (Lin et al., 2019; Zhou et al., 2018a; Wang et al., 2020a; Chen et al., 2020; Pang et al., 2019). To achieve sufficient removal of Tl(I) from high Tl-bearing wastewater, chemical oxidation of Tl and subsequent precipitation/adsorption is considered as the most feasible method (Liu et al., 2019b; Huangfu et al., 2015a).

Compared with other adsorbents, biochar produced from biomass waste is considered as a widespread and promising adsorbent with relatively large specific surface area, rich functional groups, and a low cost (Melia et al., 2019; Hu et al., 2020; Beiyuan et al., 2020). However, biochar is not conducive to separation and recycling, and the pollutant removal efficiency is limited. Therefore, magnetic nanoparticles such as Fe_3O_4 and Fe_2O_3 have been applied to prepare magnetic biochar composites, which have higher adsorption capacity and easier separation (Mohan et al., 2014; Jung et al., 2018). In recent years, $MnFe_2O_4$, due to strong magnetism, high natural abundance, and low ecotoxicity, is an attractive adsorbent (Chen et al., 2019). However, it is easy to agglomerate and not stable in the aqueous environment. Hence, impregnation of $MnFe_2O_4$ on the biochar can be used to improve the dispersion stability of $MnFe_2O_4$ and impart the magnetic properties and

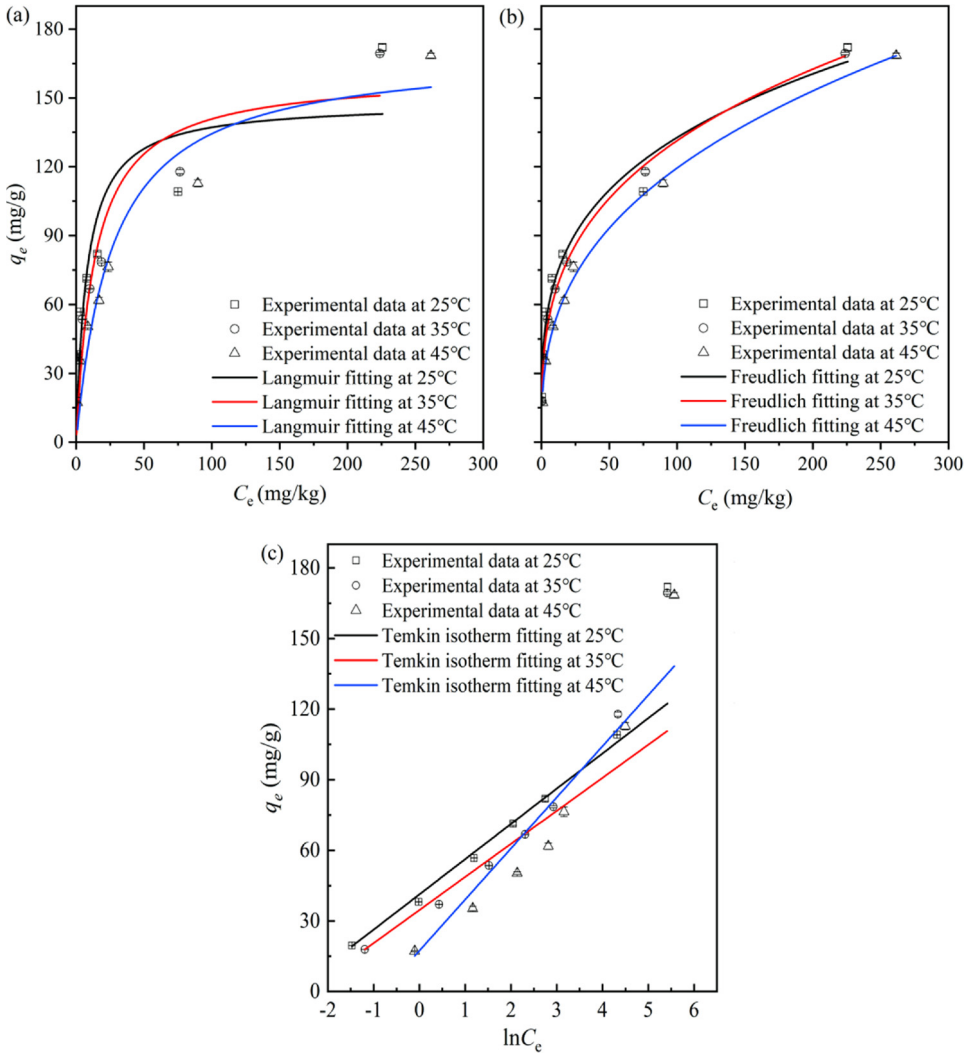

Fig. 2. Tl(I) removal by MFBC with (a) Langmuir isothermal fitting, (b) Freundlich isothermal fitting, and (c) Temkin isotherm fitting.

Table 2
Parameters of Langmuir, Freundlich and Temkin for the Tl(I) removal by MFBC.

Temperature	Langmuir model[a]			Freundlich model[b]			Temkin model[c]		
	$q_e = q_m k_L \frac{C_e}{1 + K_L C_e}$			$q_e = K_F C_e^{1/n}$			$q_e = \left(\frac{RT}{b}\right)\ln(K_T C_e)$		
	q_m	k_L	R^2	n	K_F	R^2	K_T	b	R^2
25 °C	148.00	0.127	0.830	3.654	37.633	0.976	15.777	165.500	0.996
35 °C	160.32	0.072	0.894	3.256	31.935	0.997	11.796	182.372	0.939
45 °C	170.55	0.037	0.932	2.797	23.014	0.996	2.224	121.749	0.919

[a] q_e (mg·g^{-1}) is defined as above, q_m (mg·g^{-1}) refers to the maximum removal amount of Tl. k_L (L·mg^{-1}) denotes as the Langmuir constant, C_e (mg·L^{-1}) is the concentration of Tl in a solution at equilibrium.
[b] n and K_F ((mg·g^{-1})(L·mg^{-1})$^{(1/n)}$) refer to parameters related to adsorption intensity and adsorption capacity, respectively.
[c] b (J·mol^{-1}) refers to the Temkin constant related to the heat of adsorption and K_T (L·g^{-1}) is the Temkin isotherm constant.

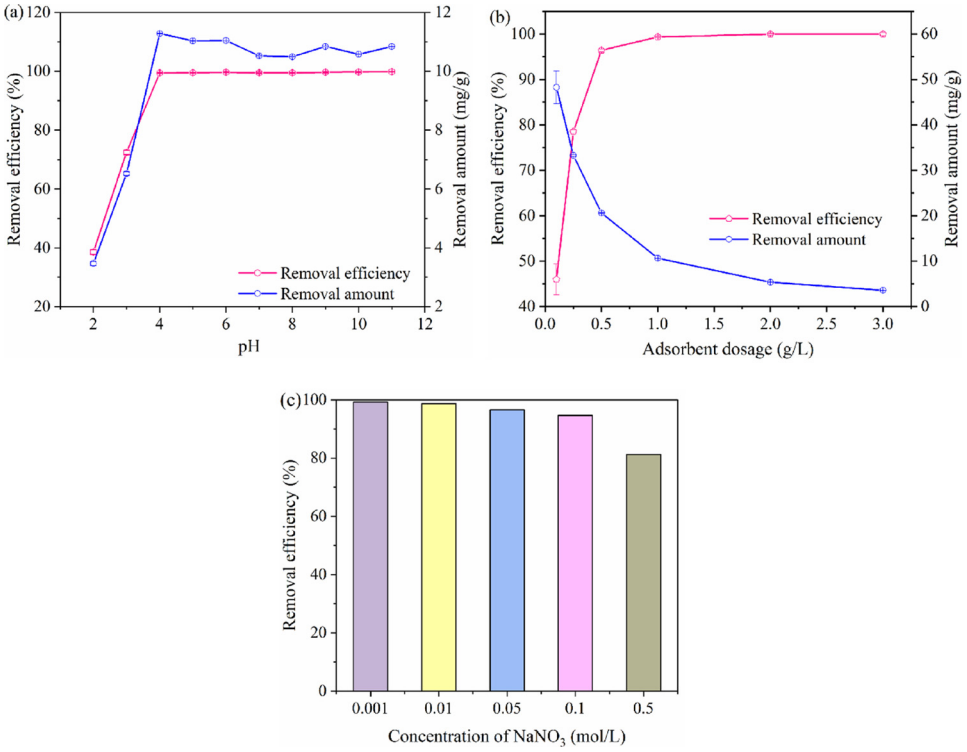

Fig. 3. Effect of (a) initial pH of solution, (b) MFBC dosage, and (c) ionic strength on Tl(I) removal by MFBC.

enhance the adsorption capacity of engineered biochar.

Herein, a $MnFe_2O_4$-biochar composite (MFBC) was prepared and used to investigate its removal of Tl(I) from wastewater. The purpose of this study was (1) to evaluate adsorption kinetics, isothermal adsorption, and crucial factors affecting adsorption (i.e., initial pH, adsorbent dosage, and ionic strength) of Tl(I) removal by the MFBC in a simulated Tl(I)-containing wastewater; and (2) to explore the removal characteristics and mechanisms of Tl(I) bound to MFBC by using various characterization techniques, such as Fourier transform infrared spectrometer (FTIR), Transmission Electron Microscopy-Energy Dispersive Spectrometer (TEM-EDS), and X-ray photoelectron spectroscopy (XPS).

2. Materials and methods

2.1. Preparation of engineered biochar

Banana leaves, which were collected from the village of Bei Ting located in Guangzhou Higher Education Mega Center of Guangzhou, China were used as precursors to prepare biochar. A slow pyrolysis process was applied to prepare biochar. Specifically, the banana leaves were rinsed and separated into petiole and blade before being oven-dried at 80 °C until constant weight. After being dried, the samples were ground by grinding miller, sieved at a size less than 0.25 mm, and stored in sealed plastic containers till further use. The pre-treated samples were pyrolyzed at 500 °C in a ceramic fiber muffle furnace under oxygen-limited conditions with a heating rate of 10 °C/min, maintained for 2 h at maximum temperature. Subsequently, the biochar was naturally cooled to room temperature, ground and passed through a 60-mesh sieve again to obtain the pristine biochar. The pristine blade biochar prepared at 500 °C was marked as BCB-500, which was used to synthesis MFBC.

2.2. Preparation of MFBC

Preparation of $MnFe_2O_4$-BC composite (MFBC) was modified following a co-precipitation method proposed by (Wang et al. (2018)). In brief, 1 g of prepared BCB-500 was mixed with 100 mL of 0.3 M iron (II) sulfate heptahydrate ($FeSO_4{\cdot}7H_2O$) solution as suspension A. Moreover, 100 mL of 0.1 M potassium permanganate ($KMnO_4$) solution was added into the suspension A with continuous stirring. Meanwhile, sodium

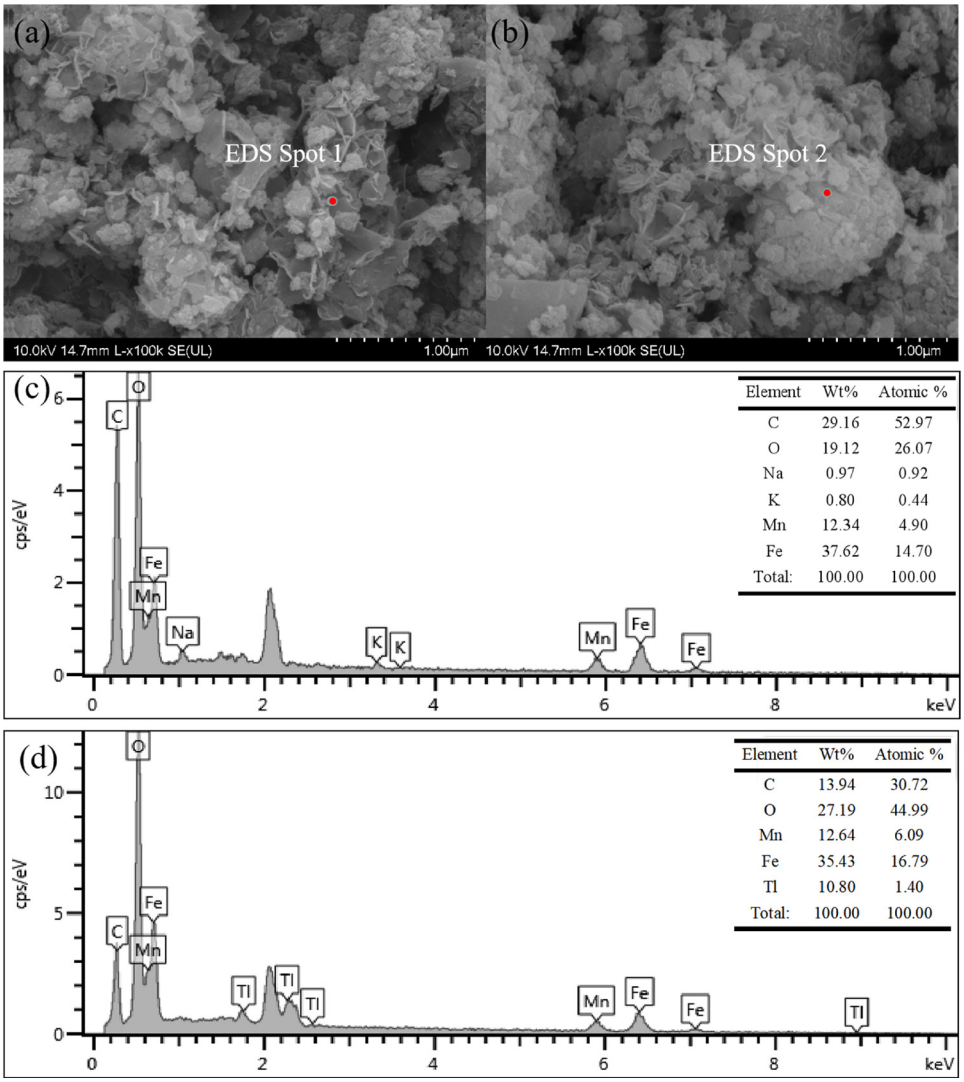

Fig. 4. SEM-EDS characterization about particles formed on MFBC: (a) and (c): before reaction, (b) and (d): after reaction with Tl(I).

hydroxide (NaOH) solution was manually added into the above-mentioned mixed solution to maintain the pH at approximately 10.0. The suspension was aged for three hours at room temperature, centrifuged and cleaned with ultra-pure water to remove excessive salts. The product was then dried under vacuum at 50 °C overnight.

2.3. Batch experiments for Tl removal using the MFBC

Thallium (I) stock solution (1000 mg/L) was prepared by dissolving $TlNO_3$ salts with ultra-pure water. The working solutions in various concentrations required in this study were obtained via further diluting the Tl(I) stock solution. The Tl concentration of all samples was determined by inductively coupled plasma-atomic emission spectrometry (ICP-OES, Avio™ 200, PerkinElmer, USA). The calibration solution was prepared by continuously diluting the high-purity ICP standard solution of Tl with ultra-pure water (18.25 Ω/cm) (Liu et al., 2018a). In order to maintain the consistency of instrument performance during the measurement process, quality control standards were run for every ten samples. The measurement accuracy was within ± 5 % RSD.

Unless stated otherwise, the conditions of adsorption experiments in this study were as follows: the initial concentration of Tl solutions was 10 mg/L, the background concentration of $NaNO_3$ solution was 0.01 mol/L, the initial pH of the reaction was 6.0, the dosage of MFBC was 1.0 g/L, the speed of oscillation was 200 r/min, the temperature of the reaction was 25 °C, contact time for adsorption experiments was 24 h. All experiments were carried out in triplicate in a 50 mL polyethylene centrifuge tube containing 25 mL Tl-bearing solution. The pH of the solutions was adjusted to the designated value by NaOH and/or HNO_3 (in various concentrations). The test results are expressed as the mean values with standard deviations.

The Tl adsorption kinetics experiments were investigated in a fixed adsorbent mass of 25 mg at different time intervals (0.5–1440 min). The Tl adsorption isotherms were studied by examining the removal of Tl with an adsorbent mass of 25 mg at various initial concentrations of Tl (I) (20–400 mg/L) at 25, 35, and 45 °C. The influence of initial pH on Tl adsorption capacity of MFBC was investigated in a range of $2-11$. The equilibrium pH values of solutions were determined after reaching the specified time. The effect of dosage (0.1–3.0 g/L) of MFBC on the removal of Tl was examined. The impact of ionic strength on the removal of Tl was also examined in 0.001, 0.01, 0.05, 0.1 and 0.5 mol/L $NaNO_3$. After reaching the adsorption reaction time, 10 mL of supernatant was obtained by filtering with 0.22-μm pore size filters. Also, 200 μL of 50 % HNO_3 was added into the filtrates for preservation and further analyses.

Tl(I) adsorption capacity (q) and removal of Tl (%) by the MFBC were obtained using Eq. (1) and Eq. (2), respectively (Pan et al., 2019; Wu et al., 2019).

$$R(\%) = \frac{(C_0 - C_e)}{C_0} \times 100 \quad (1)$$

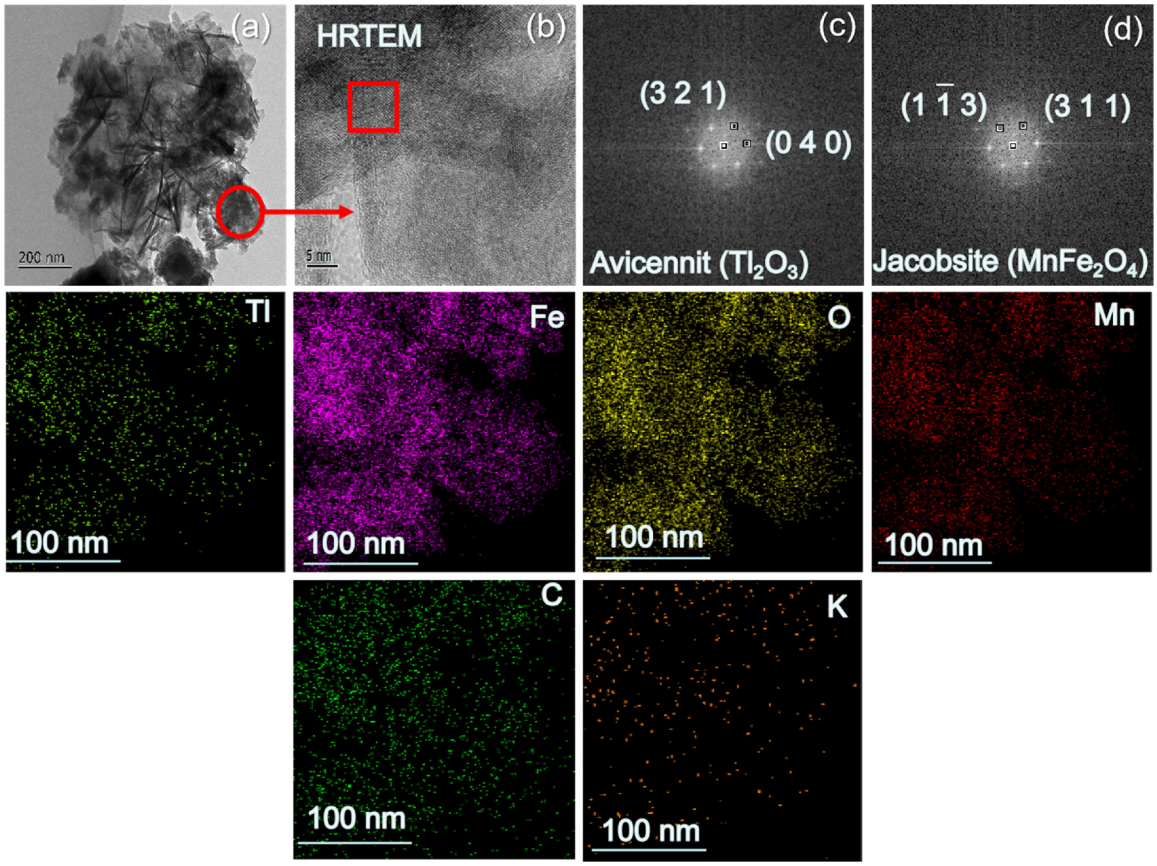

Fig. 5. TEM-EDS characterization of the MFBC after reaction with Tl(I): (a) TEM image, (b) HRTEM image; (c) SAED patterns of Tl_2O_3 and (d) SAED patterns of $MnFe_2O_4$.

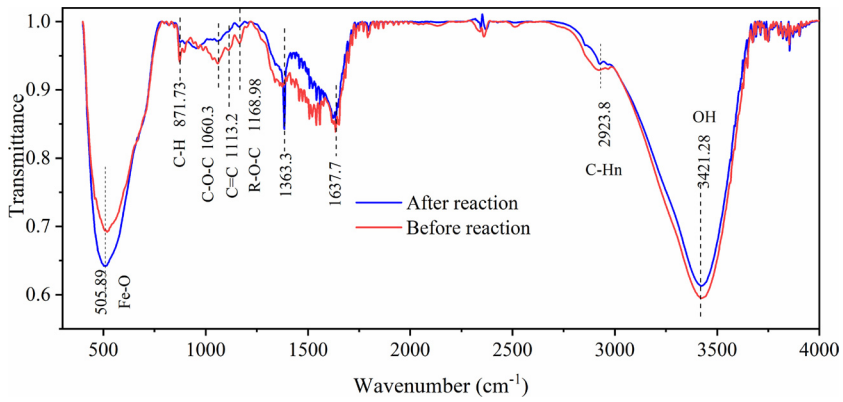

Fig. 6. FTIR characterization of the MFBC before and after reaction with Tl(I).

$$q = \frac{(C_0 - C_e) \times V}{m} \quad (2)$$

Where C_o and C_e are the initial and equilibrium concentration of Tl (mg/L), respectively. V refers to the volume of the solution (L), and m is the weight of the adsorbent (mg).

2.4. Characterization

The morphology and elemental compositions of the MFBC before and after adsorption were analyzed by a Scanning Electron Microscope (SEM, SU8220, Japan) combined with Energy Dispersive Spectrometer (EDS, Oxford) (Liu et al., 2020a). Fine structure of the MFBC was further characterized by Transmission Electron Microscopy (TEM; JEOL-2010, Japan) (Yin et al., 2019). The specific surface area (SSA) and pore-size distribution of MFBC were determined by the Brunauer–-Emmett–Teller (BET, TriStar II 3flex, USA) (Wang et al., 2018). Fourier transform infrared spectrometer (FTIR, TENSOR II+ Hyperion2000) was used to characterize the surface functional groups of the composite. X-ray photoelectron spectrometer (XPS, Thermo Scientific K-Alpha$^+$) was used to evaluate the surface composition and valence state of the composite (Liu et al., 2020a) The C1s peaks were used as the internal standard calibration peak at 284.8 eV.

3. Results and discussion

3.1. Sorption kinetics

In order to investigate the kinetics of Tl(I) sorption on MFBC,

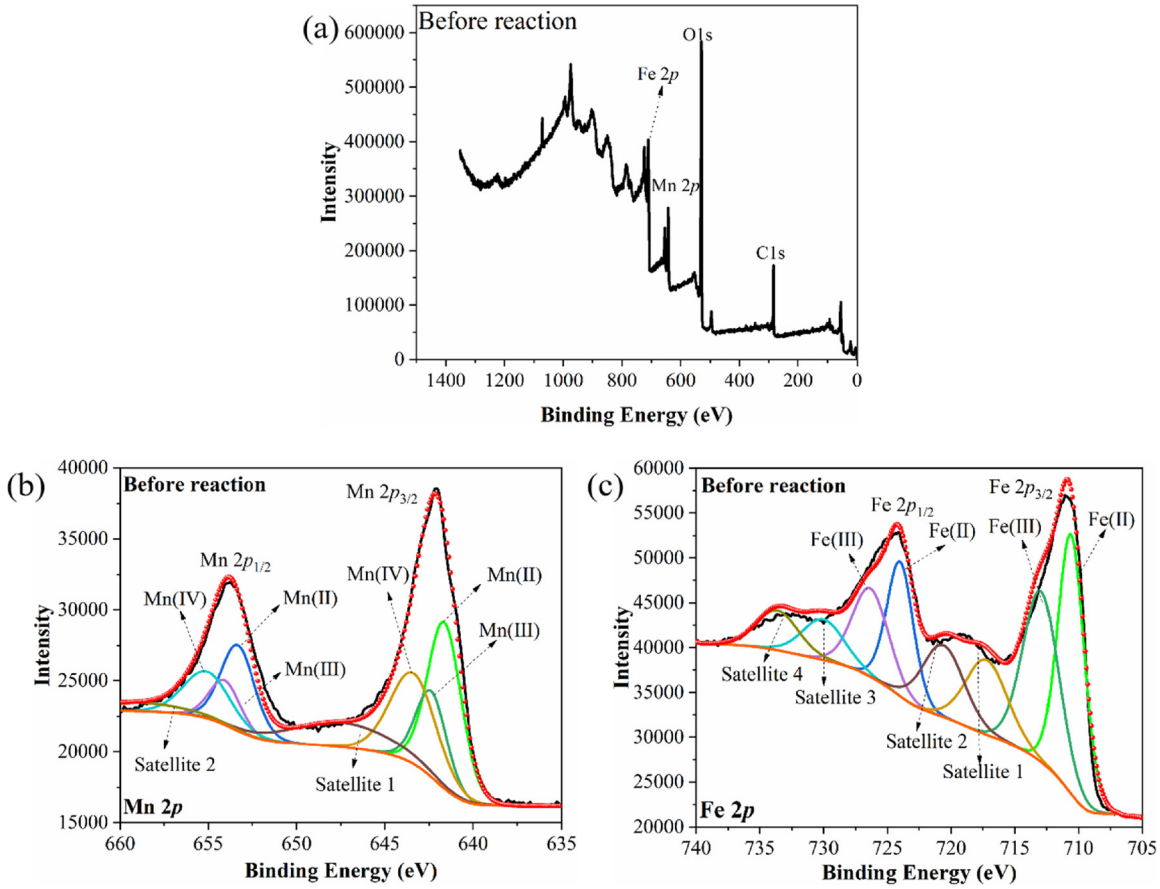

Fig. 7. XPS characterization of MFBC before reaction with Tl(I): (a) survey scan, (b) Mn 2*p* core level, (c) Fe 2*p* core level.

pseudo first order (Ho and McKay, 1998), pseudo second order (Deng et al., 2017), and intraparticle diffusion (Li et al., 2019c) models are adopted to describe the sorption process in Fig. 1a-c and the fitting parameters are given in Table 1. Tl(I) removal is characterized by a rapid removal phase in the first one minute (Fig. 1a-c), which can be attributed to the large concentration gradient force and the abundant binding sites at the early stage (Zhang et al., 2018). As the reaction progresses, the amount of binding sites and the adsorbate concentration gradually decrease, then the adsorption rate decreases with the reaction time until equilibrium. It can be observed that the correlation coefficients (R^2) of MFBC in initial Tl(I) solution(10 and 20 mg/L) were 0.9998 and 0.9990 for the pseudo first order kinetic model; and 0.9988 and 0.9985 for the pseudo second order kinetic model, respectively (Table 1). It shows that both the models can fit well with the experimental data. The calculated equilibrium Tl(I) adsorption capacities on MFBC were close to the experimental data.

To further investigate the mechanisms of adsorption kinetics, the adsorption process was studied by the intraparticle diffusion (IPD) model. The IPD model could identify the adsorption processes and assess the rate-controlling steps (Tan et al., 2015a). In this study, the IPD model can also fit well with the experimental data for the Tl(I) adsorption on MFBC (Fig. 1c), which indicates that intraparticle diffusion plays a vital role in Tl(I) adsorption. The curve can be divided into three parts, which suggests that the adsorption process has three steps (external mass transfer, intraparticle diffusion process, and adsorption/desorption equilibrium). The rate constants of MFBC decrease in the order of K_{p1}, K_{p2}, and K_{p3}, which reveals that the internal diffusion is closely related to the adsorption process. Studies have shown that if the linear curve does not traverse the origin, the intraparticle diffusion is not the rate-limiting process to control the Tl(I) adsorption rate. Meanwhile, it may involve other processes such as chemical reactions (Zhang et al., 2019a; Zhu et al., 2014).

3.2. Adsorption isotherms of MFBC

The nature of adsorption process was assessed by the investigation of adsorption isotherms (Zheng et al., 2019). The variation of the isotherms can help to infer the interactions between the adsorbate and the adsorbent and the characteristics of the adsorbed layer (Jang et al., 2018). Three widely used adsorption isotherm models of Langmuir (Zhou et al., 2018b), Freundlich (Wang et al., 2017), and Temkin (Araújo et al., 2018) were applied to shed lights on the Tl(I) sorption process on MFBC at different temperatures (25, 35 and 45 °C). Fig. 2a-c exhibit the nonlinear fitting curves of Langmuir and Freundlich isotherm models and the linear fitting curves of the Temkin model, respectively. The fitting parameters are presented in Table 2. The fitting obtained from the Freundlich isotherm model is slightly better than that from the Langmuir isotherm model. It can be inferred that the adsorption mainly occurs in multilayer and interaction between the Tl(I) and the surface of the heterogeneous composite (Zhou et al., 2018b; Tang et al., 2018). R_L (equilibrium parameter) was in the range of 0–1, indicating that adsorption is favorable. It can also be observed that the heterogeneity factor n was at the range of 2–4 at different temperatures, indicating that Tl(I) adsorption onto MFBC is facile and easy. The adsorption capacities of Tl(I) at different temperatures (25, 35 and 45 °C) were 148, 160.32, and 170.55 mg/g, respectively, which is significantly higher than those observed in other adsorbents, such as activated carbon (10.53 mg/g) (Sabermahani et al., 2017), and titanium iron magnetic adsorbent (111.3 mg/g) (Tang et al., 2019). The Temkin model also fitted the experimental data well. The regression coefficients R^2 at 25, 35 and 45 °C were 0.9958, 0.9393 and 0.9192, respectively, which suggested that MFBC has a strong internal molecular force in the

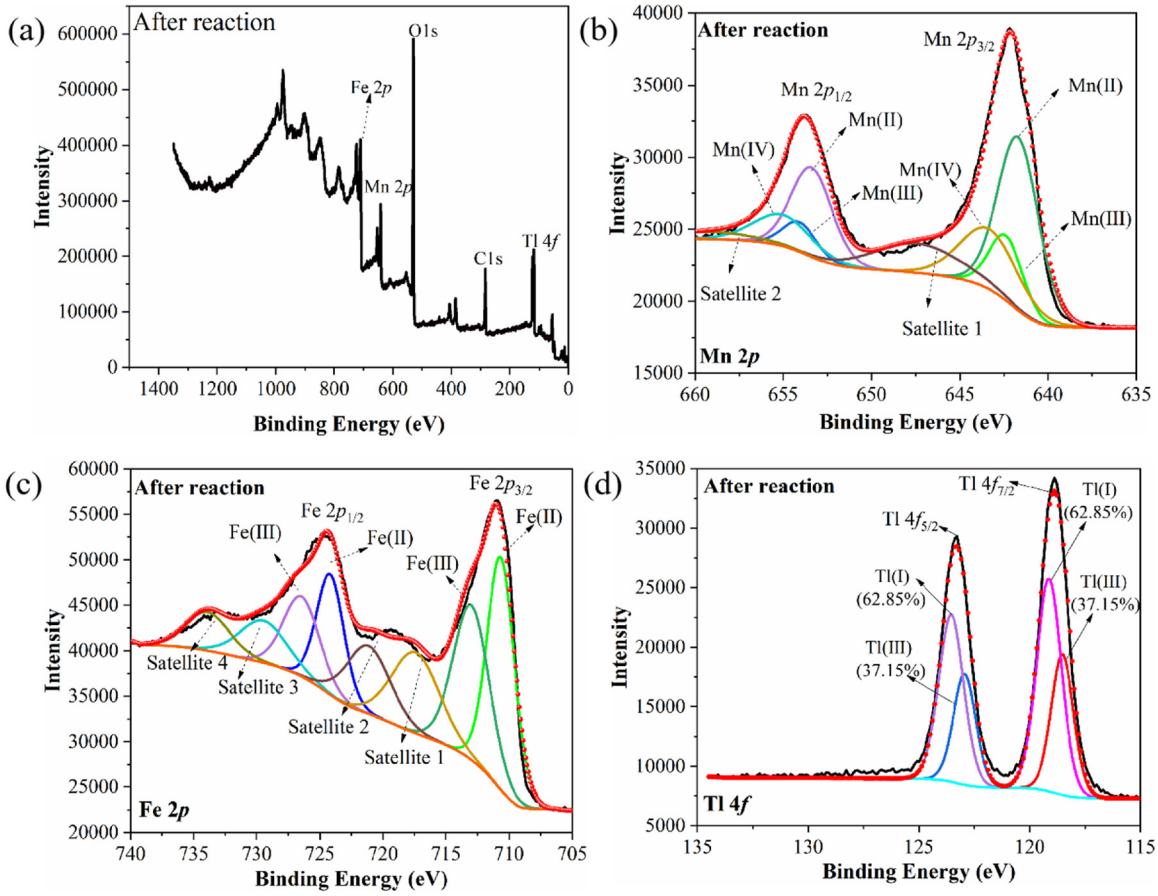

Fig. 8. XPS characterization of MFBC after reaction with Tl(I): (a) survey scan, (b) Mn 2*p* corelevel, (c) Fe 2*p* core level, (d) Tl 4*f* core level.

Tl(I) adsorption processes. According to the calculated R^2 value, the adaptability of the fitting data to the isothermal models is as follows: Freundlich > Temkin > Langmuir.

3.3. Effect of initial pH on Tl(I) removal

The solution pH is a crucial factor since it can influence the speciation of sorbate and the surface charge of adsorbent (Lai et al., 2016; Li et al., 2017c; Xiang et al., 2019a). The removal efficiencies of Tl(I) sharply increased from 38.6 to 99.4% with the initial solution pH increasing from 2 to 4. Then, the removal efficiency remained relatively constant with initial pH values ranging from pH 4–11. The removal efficiency reached a maximum value of 99.9 % under an initial pH of 11. The equilibrium pH of the solution was elevated compared to the initial pH. This may be attributed to the fact that MFBC remained alkaline after synthesis, which can neutralize the acidity in the solution, resulting in an increase of the solution pH. In general, Tl(I)-containing wastewater produced by the industrial plants is acidic. Considering the cost and removal efficiency in practical applications, pH 6 was selected as the initial pH of the solution for subsequent adsorption experiments.

3.4. Influence of adsorbent dosage on Tl removal

It can be noted from Fig. 3b that the Tl(I) removal efficiency is above 99.4 % at the adsorbent dosage of 1.0 g/L. Tl(I) can be entirely removed via MFBC at the adsorbent dosage ≥ 2.0 g/L. With an elevated dosage of MFBC, the removal efficiency of Tl(I) significantly increases, while the adsorption capacity gradually decreases (Fig. 3b). It could be ascribed to the fact that at a low MFBC dosage, the main factor limiting the increase of the removal efficiency is the available adsorption sites on the saturated MFBC. While at a higher MFBC dosage, the more available adsorption sites on MFBC contribute to the high Tl(I) removal efficiency (Zhang et al., 2019a; Zeng et al., 2018). However, adsorption sites on the accessible surface are greatly reduced as a result of MFBC accumulation, which results in a low adsorption capacity. Given the removal efficiency and experimental cost of the adsorbent, the adsorbent dosage of 1.0 g/L was selected for the following adsorption study.

3.5. Effect of ionic strength on Tl adsorption

It is crucial to examine the influence of ionic strength on the adsorption process between Tl(I) and adsorbent, as common ions usually existed in wastewater (Xiang et al., 2019b). The removal efficiency of Tl (I) decreases with increasing ionic strength, from 99.2% to 81.3% (Fig. 3c). When the concentration of $NaNO_3$ is less than 0.05 mol/L, the influence of ionic strength on Tl(I) removal was subtle. However, the ionic strength has vital effects on the Tl(I) adsorption by MFBC at high levels of $NaNO_3$ (> 0.1 mol/L) (Fig. 3c). The removal efficiency of Tl(I) was decreased with increasing ionic strength of the solution. It may be attributed to the competition between the Na^+ and Tl^+ for the available adsorption sites on MFBC (Li et al., 2017a). Secondly, the surface of the MFBC was positively charged, where NO_3^- was more readily adsorbed by electrostatic attraction. Tan et al. (2015b) and Zhang et al. (2019b) indicate that the aggregation of adsorbent particles would result in a decline in the active surface areas. This may be another reason for the reduction of the removal efficiency of Tl(I).

3.6. Characterization of MFBC

3.6.1. Morphology and microstructure characteristics

The morphology and elements percentage of the MFBC before and

after adsorption were characterized by SEM coupled with EDS, and the results are presented in Fig. 4. The coarse surface observed by SEM and the composition of the pristine sample examined by EDS (including C, O, Na, K, Mn, and Fe) indicated that $MnFe_2O_4$ particles were successfully fabricated on the pristine biochar surfaces. Especially, the C and K originate from biochar, while Fe, Mn, and O from $MnFe_2O_4$. Many small irregular particles were formed on the surface of MFBC (Fig. 4a), reflecting the Mn/Fe oxide particles generated on the biochar surface, which also was in agreement with the Mn/Fe content presented in Fig. 4c (EDS spectrum before adsorption). The uneven distribution of particle size and irregular shape may be caused by the temperature and reaction time during the preparation process.

The morphology of MFBC after adsorption was observed by the TEM (Fig. 5a) and HRTEM (Fig. 5b). Also, (311) and (113) planes (Fig. 5d) were characterized by the isometric system of $MnFe_2O_4$, which further proved the rationality in SEM-EDS analysis. This result indicates that MFBC was successfully fabricated, and the magnetism from $MnFe_2O_4$ equipped MFBC was characterized by easy separation, which is significant in practical engineering.

The results of N_2 adsorption isotherm suggest that the composite showed type IV with an H_3 hysteresis cycle (Fig. S1a). After forming $MnFe_2O_4$, the surface area of composite (187.03 m^2/g) significantly increased compared with the raw biochar (38.54 m^2/g). These may be ascribed to the formation of Mn/Fe oxide particles coupled with the activation of the surface of MFBC after modification. The significant increase in specific surface area enhances the ability of engineered biochar as an adsorbent and catalyst. Moreover, the average pore size of the modified biochar was 9.18 nm (Fig. S1b), indicating that the prepared adsorbent particles were mesoporous materials, which provided accessible adsorption sites for Tl(I).

3.6.2. Adsorption mechanisms

The EDS spectrum reveals that there was a new peaks position on the image after adsorption, which was caused by the adsorption of Tl on MFBC (Fig. 4c, d). The content of Tl on the MFBC increased after adsorption (Fig. 4c, d) confirmed that Tl was successfully adsorbed on the surface of MFBC. This is consistent with the EDS-mapping images (Fig. 5). After adsorption, the decrease of the K contents may be ascribed to ion exchange with Tl, which is contributed to the removal Tl from the solution. It can be seen from the EDS mapping that the brightness of K decreased significantly, which can illustrate the point above. Research has shown that the replacing of K^+ by Tl^+ is considered to be the main mechanism in biogeochemical reactions/cycles (Liu et al., 2018a). The identified lattice fringes from HRTEM image presented (321) and (040) planes (Fig. 5c) were characterized by the isometric system of Tl_2O_3, indicating that Tl(I) transformed to Tl (III) via the oxidation reaction in the process of adsorption. This result verified the rationality of the hypothesis from SEM-EDS analysis. Thus, as an important mechanism, oxidation plays a critical role in the Tl adsorption process.

FTIR analysis of MFBC before and after Tl(I) adsorption was investigated (Fig. 6). The peak at 505.89 cm^{-1} may be attributed to the coupling with metal O− stretch vibration, which mainly include Mn−O and FeO− before adsorption, indicating the successful incorporation of Mn/Fe oxide in the MFBC (Xiang et al., 2019b; Kumar et al., 2014). After adsorption, the signals at 505.89 cm^{-1} enhanced, which may be due to the addition of Tl-O. The peaks at 871.73 cm^{-1} might be attributed to CH− stretching in aromatic hydrogen (Li et al., 2017c). The vibration signals at 1060.3 cm^{-1}, 1113.2 cm^{-1} and 1168.98 cm^{-1} were associated with the surface functional groups C−OC/CO, CO, and HOCO−−=−=, respectively. The peak at 2923.8 cm^{-1} might be attributed to C-H_n stretching vibration in alkyl, aliphatic. The peak at 3421.28 $cm^{-1}$was associated with the stretching vibration of OH−, which may be from, in part, the adsorbed water. The signal of OH− weakened slightly after adsorption, which may be associated with the adsorption of Tl(I), indicating that iron exchange between $Tl^+$and the OH− groups on the surface of MFBC may also facilitate the removal of Tl(I) .

To further investigate the adsorption mechanism of Tl(I), XPS was applied to obtain the chemical states of MFBC before and after adsorption. The XPS spectra with the binding energies of Fe, Mn, and Tl on MFBC before and after Tl(I) adsorption were exhibited in Figs. 7 and 8, respectively. It can be observed that the presence of Fe, Mn, and O elements in the prepared MFBC sample. The Mn 2*p* spectra had a spin − orbit doublet of Mn $2p_{1/2}$ and Mn $2p_{3/2}$ (Fig. 7c). The deconvoluted Mn 2*p* spectra showed four peaks with binding energies of 641.64, 642.38, 643.39 and 647.37 eV, corresponding to Mn(II), Mn(III), Mn (IV) and satellite, respectively. It can be observed that the proportions of Mn(II), Mn(III), and Mn(IV) are 45.30%, 21.23%, and 33.47%, respectively. The main species of Mn in the MFBC is Mn(II). For the spectra of Fe 2*p*, the energy difference between Fe $2p_{1/2}$ and Fe $2p_{3/2}$ spin-orbit levels is 13.6 eV, which is consistent with the previous investigation (Li et al., 2017a). Satellite peaks of Fe(II) were detected in both Fe $2p_{1/2}$ and Fe $2p_{3/2}$ spectra, suggesting the presence of Fe(II) oxides. There are two satellite peaks of Fe(II) and Fe(III) in the Fe $2p_{1/2}$ and Fe $2p_{3/2}$ spectra of the MFBC, respectively. It indicated characteristic peaks of the oxidation states of Fe(II) and Fe(III) (Fig. 7c). This could be ascribed to part of Fe(II) being adsorbed on biochar during the synthesis of materials.

After adsorption, Mn(II) was increased by about 10 %. It could be explained by that part of Mn(III) and Mn(IV) were reduced to Mn(II) after Tl(I) adsorption. The peak of Tl 4*f* appeared, indicating that Tl(I) was adsorbed on the surfaces of the MFBC (Fig. 8d), which is consistent with the results of EDS elemental mapping in Fig. 5. The Tl 4*f* spectra with the binding energy of 118.5 eV (Wan et al., 2014) and 119.1 eV (Tang et al., 2019) indicate peaks with characteristics of Tl(III) and Tl(I) oxidation states (Fig. 8d). This also agrees with the observation in HRTEM (Fig. 5). The peak of Tl(III) was found in Tl 4*f* spectra of MFBC after Tl(I) adsorption, which suggests that the oxidation state of Tl(I) can be altered in the process of adsorption on the MFBC. Among them, approximate 37.15% of Tl(I) captured by MFBC was oxidized to Tl(III). Since Tl(III) is unstable and easily reduced in the air, it may lead to an underestimation of Tl(III) contents detected by XPS (Peter and Viraraghavan, 2005). Therefore, oxidation could be designated as a principal mechanism for Tl(I) removal by the MFBC. Besides, it is observed that no apparent difference in Fe 2*p* spectrum after the adsorption of Tl(I), indicating that the valence state of Fe in the adsorbent did not change in the adsorption process (Fig. 8). In addition, ion exchange may also be another main driving force in the adsorption process. It can be described as Eq. (3) and Eq. (4).

$$-Mn-OH+Tl^{+}\Leftrightarrow Mn-O-Tl+H^{+} \quad (3)$$

$$-Fe-OH+Tl^{+}\Leftrightarrow Fe-O-Tl+H^{+} \quad (4)$$

4. Conclusions

In summary, MFBC manifests an excellent performance in the removal of Tl(I) under a wide range of pH from the Tl(I)-containing wastewater, and the maximum removal capacity reached 170.55 mg/g. The ionic strength has a significant effect on the Tl(I) removal by MFBC at high levels of $NaNO_3$. The experimental data can be well fitted with the pseudo-first-order, pseudo-second-order kinetic model, and intraparticle diffusion models, while the adsorption isotherm can be well described by Freundlich and Temkin isotherm models. Physical and chemical adsorption, ion exchange, surface complexation, and oxidation are the main mechanisms for the Tl(I) removal. Hence, MFBC is a promising and environmentally friendly adsorbent for the Tl(I) removal in aqueous solution.

CRediT authorship contribution statement

Juan Liu: Writing - original draft, Methodology, Investigation, Visualization, Funding acquisition. **Shixing Ren:** Formal analysis, Investigation, Writing - review & editing. **Jielong Cao:** Writing - review & editing. **Daniel C.W. Tsang:** Writing - review & editing. **Jingzi Beiyuan:** Writing - review & editing. **Yutao Peng:** Writing - review & editing. **Fa Fang:** Writing - review & editing, Writing - review & editing. **Jingye She:** Writing - review & editing. **Meiling Yin:** Writing - review & editing. **Nengping Shen:** Writing - review & editing. **Jin Wang:** Supervision, Project administration, Writing - review & editing.

Declaration of Competing Interest

The authors declare that they have no known competing financial interests or personal relationships that could have appeared to influence the work reported in this paper.

Acknowledgement

The work was funded by the Natural Science Foundation of China (Nos. 41873015, 41830753, U1612442, 41573008 and 41773011), the Guangzhou University's 2017 training program for young top-notch personnel (BJ201709), Scientific Research Projects in Colleges and Universities of Guangzhou Education Bureau, Guangzhou, China (201831803), and the 17th "Challenge Cup" Undergraduate Program (team leader: Jielong Cao).

Appendix A. Supplementary data

Supplementary material related to this article can be found, in the online version, at doi:https://doi.org/10.1016/j.jhazmat.2020.123311.

References

Adio, S.O., Asif, M., Mohammed, A.-R.I., Baig, N., Al-Arfaj, A.A., Saleh, T.A., 2019. Poly (amidoxime) modified magnetic activated carbon for chromium and thallium adsorption: statistical analysis and regeneration. Process. Saf. Environ. Prot. 121, 254–262.

L. Albert, H. Masson, Thallium extraction process. United States Patent 529604, (1994), Metaleurop S.A, France.

Araújo, C.S., Almeida, I.L., Rezende, H.C., Marcionilio, S.M., Léon, J.J.L., Matos, T.N., 2018. Elucidation of mechanism involved in adsorption of Pb (II) onto lobeira fruit (Solanum lycocarpum) using Langmuir, Freundlich and Temkin isotherms. Microchem. J. 137, 348–354.

Beiyuan, J., Awad, Y.M., Beckers, F., Wang, J., Tsang, D.C.W., Ok, Y.S., Wang, S.-L., Wang, H., Rinklebe, J., 2020. (Im)mobilization and speciation of lead under dynamic redox conditions in a contaminated soil amended with pine sawdust biochar. Environ. Int. 135, 105376.

Birungi, Z.S., Chirwa, E.M.N., 2015. The adsorption potential and recovery of thallium using green micro-algae from eutrophic water sources. J. Hazard. Mater. 299, 67–77.

Chen, Q., Zheng, J., Yang, Q., Dang, Z., Zhang, L., 2019. Insights into the glyphosate adsorption behavior and mechanism by a MnFe2O4@Cellulose-Activated carbon magnetic hybrid. ACS Appl. Mater. Interfaces 11, 15478–15488.

Chen, Z., Zhang, S., Liu, Y., Alharbi, N.S., Rabah, S.O., Wang, S., Wang, X., 2020. Synthesis and fabrication of g-C3N4-based materials and their application in elimination of pollutants. Sci. Total Environ. 731, 139054.

Deng, J., Liu, Y., Liu, S., Zeng, G., Tan, X., Huang, B., Tang, X., Wang, S., Hua, Q., Yan, Z., 2017. Competitive adsorption of Pb(II), Cd(II) and Cu(II) onto chitosan-pyromellitic dianhydride modified biochar. J. Colloid Interface Sci. 506, 355–364.

George, L.L., Biagioni, C., Lepore, G.O., Lacalamita, M., Agrosi, G., Capitani, G.C., Bonaccorsi, E., d'Acapito, F., 2019. The speciation of thallium in (Tl, Sb, As)-rich pyrite. Ore Geol. Rev. 107, 364–380.

Ho, Y.-S., McKay, G.J., 1998. A comparison of chemisorption kinetic models applied to pollutant removal on various sorbents. Process. Saf. Environ. Prot. 76 (1998), 332–340.

Hu, B., Ai, Y., Jin, J., Hayat, T., Alsaedi, A., Zhuang, L., Wang, X., 2020. Efficient elimination of organic and inorganic pollutants by biochar and biochar-based materials. Biochar 2, 47–64.

Huangfu, X., Jiang, J., Lu, X., Wang, Y., Liu, Y., Pang, S.-Y., Cheng, H., Zhang, X., Ma, J., 2015a. Adsorption and oxidation of thallium(I) by a nanosized manganese dioxide. Water Air Soil Pollut. 226.

Jang, H.M., Yoo, S., Choi, Y.-K., Park, S., Kan, E., 2018. Adsorption isotherm, kinetic modeling and mechanism of tetracycline on Pinus taeda-derived activated biochar. Bioresour. Technol. Rep. 259, 24–31.

Jung, K.W., Lee, S.Y., Lee, Y.J., 2018. Facile one-pot hydrothermal synthesis of cubic spinel-type manganese ferrite/biochar composites for environmental remediation of heavy metals from aqueous solutions. Bioresour. Technol. Rep. 261, 1–9.

Kumar, S., Nair, R.R., Pillai, P.B., Gupta, S.N., Iyengar, M.A., Sood, A.K., 2014. Graphene oxide-$MnFe_2O_4$ magnetic nanohybrids for efficient removal of lead and arsenic from water. ACS Appl. Mater. Interfaces 6, 17426–17436.

Lai, C., Wang, M.-M., Zeng, G.-M., Liu, Y.-G., Huang, D.-L., Zhang, C., Wang, R.-Z., Xu, P., Cheng, M., Huang, C., Wu, H.-P., Qin, L., 2016. Synthesis of surface molecular imprinted TiO2/graphene photocatalyst and its highly efficient photocatalytic degradation of target pollutant under visible light irradiation. Appl. Surf. Sci. 390, 368–376.

Li, H., Chen, Y., Long, J., Li, X., Jiang, D., Zhang, P., Qi, J., Huang, X., Liu, J., Xu, R., Gong, J., 2017a. Removal of thallium from aqueous solutions using Fe-Mn binary oxides. J. Hazard. Mater. 338, 296–305.

Li, H., Chen, Y., Long, J., Jiang, D., Liu, J., Li, S., Qi, J., Zhang, P., Wang, J., Gong, J., Wu, Q., Chen, D., 2017b. Simultaneous removal of thallium and chloride from a highly saline industrial wastewater using modified anion exchange resins. J. Hazard. Mater. 333, 179–185.

Li, B., Yang, L., Wang, C.Q., Zhang, Q.P., Liu, Q.C., Li, Y.D., Xiao, R., 2017c. Adsorption of Cd(II) from aqueous solutions by rape straw biochar derived from different modification processes. Chemosphere 175, 332–340.

Li, N., Yin, M., Tsang, D.C.W., Yang, S., Liu, J., Li, X., Song, G., Wang, J., 2019c. Mechanisms of U(VI) removal by biochar derived from Ficus microcarpa aerial root: a comparison between raw and modified biochar. Sci. Total Environ. 697.

Li, N., Zhou, Y., Liu, J., Tsang, D., Wang, J., She, J., Zhou, Y., Yin, M., Chen, Z., Chen, D., 2020. Persistent thallium contamination in river sediments, source apportionment and environmental implications. Ecotoxicol. Environ. Saf. 202, 110874.

Lin, L., Song, Z., Khan, Z.H., Liu, X., Qiu, W., 2019. Enhanced As (III) removal from aqueous solution by Fe-Mn-La-impregnated biochar composites. Sci. Total Environ. 686, 1185–1193.

Liu, W., Zhang, P., Borthwick, A.G.L., Chen, H., Ni, J., 2014a. Adsorption mechanisms of thallium(I) and thallium(III) by titanate nanotubes: ion-exchange and co-precipitation. J. Colloid Interface Sci. 423, 67–75.

Liu, W., Zhang, P., Borthwick, A.G., Chen, H., Ni, J., 2014b. Adsorption mechanisms of thallium (I) and thallium (III) by titanate nanotubes: ion-exchange and co-precipitation. J. Colloid Interface Sci. 423, 67–75.

Liu, J., Wang, J., Xiao, T., Bao, Za., Lippold, H., Luo, X., Yin, M., Ren, J., Chen, Y., Linghu, W., 2018a. Geochemical dispersal of thallium and accompanying metals in sediment profiles from a smelter-impacted area in South China. Appl. Geochem. 88, 239–246.

Liu, J., Wang, J., Tsang, D.C.W., Xiao, T., Chen, Y., Hou, L., 2018b. Emerging thallium pollution in China and source tracing by thallium isotopes. Environ. Sci. Technol. 52, 11977–11979.

Liu, J., Li, N., Zhang, W., Wei, X., Tsang, D.C.W., Sun, Y., Luo, X., Bao, Za., Zheng, W., Wang, J., Xu, G., Hou, L., Chen, Y., Feng, Y., 2019a. Thallium contamination in farmlands and common vegetables in a pyrite mining city and potential health risks. Environ. Pollut. 248, 906–915.

Liu, J., Luo, X., Sun, Y., Tsang, D.C.W., Qi, J., Zhang, W., Li, N., Yin, M., Wang, J., Lippold, H., Chen, Y., Sheng, G., 2019b. Thallium pollution in China and removal technologies for waters: a review. Environ. Int. 126, 771–790.

Liu, J., Ren, S., Zhou, Y., Tsang, D., Lippold, H., Wang, J., Yin, M., Xiao, T., Luo, X., Chen, Y., 2019c. High contamination risks of thallium and associated metal(loid)s in fluvial sediments from a steel-making area and implications for environmental management. J. Environ. Manage. 250, 109513.

Liu, J., Ren, J., Zhou, Y., Tsang, D.C.W., Lin, J., Yuan, W., Wang, J., Yin, M., Wu, Y., Xiao, T., Chen, Y., 2020a. Effects and mechanisms of mineral amendment on thallium mobility in highly contaminated soils. J. Environ. Manage. 262, 110251.

Liu, J., Yin, M., Xiao, T., Zhang, C., Tsang, D., Bao, Z., Zhou, Y., Chen, Y., Luo, X., Yuan, W., Wang, J., 2020b. Thallium isotopic fractionation in industrial process of pyrite smelting and environmental implications. J. Hazard. Mater. 384, 121378.

Liu, J., Wei, X., Zhou, Y., Tsang, D., Bao, Z., Yin, M., Lippold, H., Yuan, W., Wang, J., Feng, Y., Chen, D., 2020c. Thallium contamination, health risk assessment and source apportionment in common vegetables. Sci. Total Environ. (703), 135547.

Martin, L.A., Wissocq, A., Benedetti, M.F., Latrille, C., 2018. Thallium (Tl) sorption onto illite and smectite: implications for Tl mobility in the environment. Geochim. Cosmochim. Acta 230, 1–16.

Melia, P.M., Busquets, R., Hooda, P.S., Cundy, A.B., Sohi, S.P., 2019. Driving forces and barriers in the removal of phosphorus from water using crop residue, wood and sewage sludge derived biochars. Sci. Total Environ. 675, 623–631.

Mohan, D., Sarswat, A., Ok, Y.S., Pittman Jr., C.U., 2014. Organic and inorganic contaminants removal from water with biochar, a renewable, low cost and sustainable adsorbent–a critical review. Bioresour. Technol. Rep. 160, 191–202.

Pan, B., Wan, S., Zhang, S., Guo, Q., Xu, Z., Lv, L., Zhang, W., 2014. Recyclable polymer-based nano-hydrous manganese dioxide for highly efficient Tl(I) removal from water. Sci. China-Chem. 57, 763–771.

Pan, N., Jin, Y., Wang, X., Hu, X., Chi, F., Zou, H., Xia, C., 2019. A Self-Assembled Supramolecular Material Containing Phosphoric Acid for Ultrafast and Efficient Capture of Uranium from Acidic Solutions. ACS Sustain. Chem. Eng. 7 (1), 950–960.

Pang, H., Wu, Y., Wang, X., Hu, B., Wang, X., 2019. Recent advances in composites of graphene and layered double hydroxides for water remediation: a review. Chem. An Asian J. 14, 2542–2552.

Peter, A.L.J., Viraraghavan, T., 2005. Thallium: a review of public health and environmental concerns. Environ. Int. 31, 493–501.

Puccini, M., Guazzelli, L., Tasca, A.L., Mezzetta, A., Pomelli, C.S., 2018. Development of a chemosensor for the in situ monitoring of thallium in the water network. Water Air Soil Pollut. 229.

Sabermahani, F., Mahani, N.M., Noraldiny, M., 2017. Removal of thallium (I) by

activated carbon prepared from apricot nucleus shell and modified with rhodamine B. Toxin Rev. 36, 154–160.
Saleh, T.A., Tuzen, M., Sari, A., 2018. Polyamide magnetic palygorskite for the simultaneous removal of Hg(II) and methyl mercury; with factorial design analysis. J. Environ. Manage. 211, 323–333.
Tan, X., Liu, Y., Zeng, G., Wang, X., Hu, X., Gu, Y., Yang, Z., 2015a. Application of biochar for the removal of pollutants from aqueous solutions. Chemosphere 125, 70–85.
Tan, L., Wang, Y., Liu, Q., Wang, J., Jing, X., Liu, L., Liu, J., Song, D., 2015b. Enhanced adsorption of uranium (VI) using a three-dimensional layered double hydroxide/graphene hybrid material. Chem. Eng. J. 259, 752–760.
Tang, L., Yu, J., Pang, Y., Zeng, G., Deng, Y., Wang, J., Ren, X., Ye, S., Peng, B., Feng, H., 2018. Sustainable efficient adsorbent: alkali-acid modified magnetic biochar derived from sewage sludge for aqueous organic contaminant removal. Chem. Eng. J. 336, 160–169.
Tang, J., Wu, W., Yu, L., Fan, X., Liu, G., Yu, Y., 2019. Study on adsorption properties and mechanism of thallium onto titanium-iron magnetic adsorbent. Sci. Total Environ. 694, 133625.
Tuzen, M., Sari, A., Saleh, T.A., 2018. Response surface optimization, kinetic and thermodynamic studies for effective removal of rhodamine B by magnetic AC/CeO_2 nanocomposite. J. Environ. Manage. 206, 170–177.
Vaněk, A., Chrastný, V., Komárek, M., Penížek, V., Teper, L., Cabala, J., Drábek, O., 2013. Geochemical position of thallium in soils from a smelter-impacted area. J. Geochem. Explor. 124, 176–182.
Vanek, A., Grosslova, Z., Mihaljevic, M., Trubac, J., Ettler, V., Teper, L., Cabala, J., Rohovec, J., Zadorova, T., Penizek, V., Pavlu, L., Holubik, O., Nemecek, K., Houska, J., Drabek, O., Ash, C., 2016. Isotopic tracing of thallium contamination in soils affected by emissions from coal-fired power plants. Environ. Sci. Technol. 50, 9864–9871.
Vanek, A., Holubik, O., Oborna, V., Mihaljevic, M., Trubac, J., Ettler, V., Pavlu, L., Vokurkova, P., Penizek, V., Zadorova, T., Voegelin, A., 2019. Thallium stable isotope fractionation in white mustard: implications for metal transfers and incorporation in plants. J. Hazard. Mater. 369, 521–527.
Vink, B.J.C.G., 1993. The behaviour of thallium in the (sub) surface environment in terms of Eh and pH. Chem. Geol. 109, 119–123.
Wan, S., Ma, M., Lv, L., Qian, L., Xu, S., Xue, Y., Ma, Z., 2014. Selective capture of thallium(I) ion from aqueous solutions by amorphous hydrous manganese dioxide. Chem. Eng. J. 239, 200–206.
Wang, S., Gao, B., Li, Y., Creamer, A.E., He, F., 2017. Adsorptive removal of arsenate from aqueous solutions by biochar supported zero-valent iron nanocomposite: batch and continuous flow tests. J. Hazard. Mater. 322, 172–181.
Wang, Y.-Y., Ji, H.-Y., Lu, H.-H., Liu, Y.-X., Yang, R.-Q., He, L.-L., Yang, S.-M., 2018. Simultaneous removal of Sb(III) and Cd(II) in water by adsorption onto a MnFe2O4–biochar nanocomposite. RSC Adv. 8, 3264–3273.
Wang, X., Li, X., Wang, J., Zhu, H., 2020a. Recent advances in carbon nitride-based nanomaterials for the removal of heavy metal ions from aqueous solution. J. Inorg. Mater. 35, 260–270.
Wang, J., She, J., Zhou, Y., Tsang, D.C.W., Beiyuan, J., Xiao, T., Dong, X., Chen, Y., Liu, J., Yin, M., Wang, L., 2020b. Microbial insights into the biogeochemical features of thallium occurrence: A case study from polluted river sediments. Sci. Total Environ., 139957.
Wang, J., Zhou, Y., Dong, X., Yin, M., Tsang, D., Sun, J., Liu, J., Song, G., Liu, Y., 2020c. Temporal sedimentary record of thallium pollution in an urban lake: An emerging thallium pollution source from copper metallurgy. Chemosphere 242, 125172.
Wang, J., Jiang, Y., Sun, J., She, J., Yin, M., Fang, F., Xiao, T., Song, G., Liu, J., 2020d. Geochemical transfer of cadmium in river sediments near a lead-zinc smelter. Ecotoxicol. Environ. Saf. 196, 110529.
Wojtkowiak, T., Karbowska, B., Zembrzuski, W., Siepak, M., Lukaszewski, Z., 2016. Miocene colored waters: a new significant source of thallium in the environment. J. Geochem. Explor. 161, 42–48.
Wu, Y., Chen, D., Kong, L., Tsang, D.C.W., Su, M., 2019. Rapid and effective removal of uranium (VI) from aqueous solution by facile synthesized hierarchical hollow hydroxyapatite microspheres. J. Hazard. Mater. 371, 397–405.
Xiang, Y., Xu, Z., Wei, Y., Zhou, Y., Yang, X., Yang, Y., Yang, J., Zhang, J., Luo, L., Zhou, Z.J.Joem., 2019a. Carbon-based materials as adsorbent for antibiotics removal: mechanisms and influencing factors. J. Environ. Manage. 237, 128–138.
Xiang, Y., Xu, Z., Zhou, Y., Wei, Y., Long, X., He, Y., Zhi, D., Yang, J., Luo, L., 2019b. A sustainable ferromanganese biochar adsorbent for effective levofloxacin removal from aqueous medium. Chemosphere 237, 124464.
Xiao, T., Yang, F., Li, S., Zheng, B., Ning, Z., 2012. Thallium pollution in China: a geo-environmental perspective. Sci. Total Environ. 421-422, 51–58.
Yin, M., Sun, J., Chen, Y., Wang, J., Shang, J., Belshaw, N., Shen, C., Liu, J., Li, H., Linghu, W., Xiao, T., Dong, X., Song, G., Xiao, E., Chen, D., 2019. Mechanism of uranium release from uranium mill tailings under long-term exposure to simulated acid rain: Geochemical evidence and environmental implication. Environ. Pollut. 244, 174–181.
Yin, M., Tsang, D., Sun, J., Wang, J., Shang, J., Fang, F., Liu, J., Song, G., Xiao, T., Chen, D., 2020. Critical insight and indication on particle size effects towards uranium release from uranium mill tailings: Geochemical and mineralogical aspects. Chemosphere 250, 126315.
Zeng, J., Han, G., 2020. Preliminary copper isotope study on particulate matter in Zhujiang River, Southwest China: Application for source identification. Ecotoxicol. Environ. Saf. 198, 110663.
Zeng, Z.W., Tan, X.F., Liu, Y.G., Tian, S.R., Zeng, G.M., Jiang, L.H., Liu, S.B., Li, J., Liu, N., Yin, Z.H., 2018. Comprehensive adsorption studies of doxycycline and ciprofloxacin antibiotics by biochars prepared at different temperatures. Front. Chem. 6, 80.
Zhang, G., Fan, F., Li, X., Qi, J., Chen, Y., 2018. Superior adsorption of thallium(I) on titanium peroxide: performance and mechanism. Chem. Eng. J. 331, 471–479.
Zhang, P., Li, Y., Cao, Y., Han, L., 2019a. Characteristics of tetracycline adsorption by cow manure biochar prepared at different pyrolysis temperatures. Bioresour. Technol. 285.
Zhang, S., Lyu, H., Tang, J., Song, B., Zhen, M., Liu, X., 2019b. A novel biochar supported CMC stabilized nano zero-valent iron composite for hexavalent chromium removal from water. Chemosphere 217, 686–694.
Zheng, N., Yin, L., Su, M., Liu, Z., Tsang, D.C., Chen, D., 2020. Synthesis of shape and structure-dependent hydroxyapatite nanostructures as a superior adsorbent for removal of U (VI). Chem. Eng. J. 384, 123262.
Zhong, Q., Zhou, Y., Tsang, C.W.D., Liu, J., Yang, X., Yin, M., Wu, S., Wang, J., Xiao, T., Zhang, Z., 2020. Cadmium isotopes as tracers in environmental studies: A review. Sci. Total Environ. 736, 139585.
Zhou, Q., Lin, L., Qiu, W., Song, Z., Liao, B., 2018a. Supplementation with ferromanganese oxide–impregnated biochar composite reduces cadmium uptake by indica rice *(Oryza sativa* L.). J. Clean. Prod. 184, 1052–1059.
Zhou, Q., Liao, B., Lin, L., Qiu, W., Song, Z., 2018b. Adsorption of Cu(II) and Cd(II) from aqueous solutions by ferromanganese binary oxide-biochar composites. Sci. Total Environ. 615, 115–122.
Zhou, Y., Wang, L., Xiao, T., Chen, Y., Beiyuan, J., She, J., Zhou, Y., Yin, M., Liu, J., Liu, Y., Wang, Y., Wang, J., 2020. Legacy of multiple heavy metal(loid)s contamination and ecological risks in farmland soils from a historical artisanal zinc smelting area. Sci. Total Environ. 720, 137541.
Zhu, X., Liu, Y., Qian, F., Zhou, C., Zhang, S., Chen, J., 2014. Preparation of magnetic porous carbon from waste hydrochar by simultaneous activation and magnetization for tetracycline removal. Bioresour. Technol. 154, 209–214.